



## Toward a facile synthesis of spherical sub-micron mesoporous silica: Effect of surfactant concentration

Seyed Omid Reza Sheykhholeslami, Mohamadreza Etminanfar\*, Jafar Khalil-Allafi

Research Center for Advanced Materials, Faculty of Materials Engineering, Sahand University of Technology, Tabriz, Iran.

Received: 19 May 2020; Accepted: 8 June 2020

\* Corresponding author email: [etminanfar@sut.ac.ir](mailto:etminanfar@sut.ac.ir)

### ABSTRACT

In this paper, a facile method for preparing sub-micron spherical mesoporous silica by the sol-gel process and cationic surfactant cetyltrimethylammonium bromide (CTAB) as a soft template was reported. Moreover, the effect of surfactant concentration on the specific surface area and the total pore volume was investigated. The specific surface area, pore characteristic, morphology, chemical composition, and structure of mesoporous silica were studied using various methods. The  $N_2$  adsorption test showed that increasing the CTAB concentration from 4.6 mM to 7.2 mM increases the specific surface area from 416.48 to 564.07  $m^2g^{-1}$ . However, the maximum pore volume was obtained at 5.9 mM CTAB. The spherical shape of the powders was confirmed by field emission scanning electron microscopy. Besides, X-ray diffraction, fourier transform infrared spectra, and energy dispersive spectrometry analysis indicated that the synthesized samples are  $SiO_2$ , with an amorphous structure. Based on the structure and properties of obtained synthesized mesoporous silica, it is a good candidate for a drug reservoir and the carrier for new controlled drug delivery systems.

**Keywords:** Mesoporous, Silica, Surfactant, CTAB, Specific surface area, Pore volume.

### 1. Introduction

One of the most promising ways to improve human health is using controlled drug delivery systems (DDSs) [1]. Generally, DDSs can control the rate and the period of drug release and targets specific areas of the body. On the other hand, traditional methods increase the drug concentration in blood plasma suddenly, and then the concentration of drug rapidly decreases in the same way as a saw-tooth curve [2]. Furthermore, most hydrophobic drugs have limited use because of their low water solubility, resulting in weak gastrointestinal absorption after oral dosing. The DDSs can resolve this disadvantage of oral consumption of drugs [3].

Porous materials have attracted attention in many functional areas, like optics [4], energy [5], electronics [6], medical [7], and biotechnological [8] applications. This is due to their adsorption, storage, and release properties because of a high surface area and pore volume. Based on the international union of pure and applied chemistry (IUPAC), porous materials are classified into three groups depending on their pore sizes: microporous, mesoporous, macroporous materials with pore size  $<2$  nm, 2-50 nm, and  $>50$  nm, respectively [9-11]. The zeolites are the most well-known microporous materials which have excellent catalytic properties. But the fine pore size of the materials has limited their applications in some fields like drug delivery.

Therefore, the mesoporous materials received more attention in this field due to the appropriate pore size [12].

There are two different pathways to synthesize the mesoporous materials, including soft-templating and hard-templating [13]. In the hard-templating method, a porous solid like silica or carbon is used as the template instead of a surfactant [14,15]. In the soft-templating route, there are typically three steps to form a mesoporous material. In the first step, the surfactant is self-organized; in the second stage, the inorganic precursor is organized over this surfactant, and a stable inorganic-organic composite is formed. At last, the organic template is removed to get the mesoporous materials [16].

Studies have shown that there are two main mechanisms for the formation of inorganic-surfactant composite materials in the soft-templating route, including cooperative self-assembly (CSA) and "true" liquid-crystal templating (TLCL) [17]. In the CSA mechanism, self-organized templates simultaneously aggregate with inorganic species, and a liquid-crystal phase containing the organic micelle and inorganic precursor could be created [15]. The TLCL mechanism proposed for the first time by Mobil corporation laboratories. In this method, the concentration of the surfactant is very high. So that, a liquid-crystalline phase is formed under the dominant conditions (temperature, pH) without the precursor inorganic framework materials [15,18].

In recent years, the mesoporous silica has shown a great interest in the field of medicine. The key advantages of mesoporous silica are simple, scalable, and cost-effective manufacturing. Besides, its non-toxic matrix structure, large surface area, and pore volume are vulnerable to functionality [19,20]. Vallet-Regi et al. in 2001, proposed the mesoporous silica for the drug delivery system [21]. Silica is a bioactive ceramics that plays a significant role in the metabolism of connective tissue [22]. Furthermore, biodegradation is one of the prerequisites for design in pharmacy. Silica is absorbed into the blood circulation by the reticulo-endothelial system and is degraded by the urine before excretion [23].

The pore diameters of mesoporous silica are usually about 2-3 nm [24]. Therefore, preparing mesoporous silica with a large pore size for storage a high amount of the drug molecule and different types of drugs is highly desired. The main objective of the current study is to synthesize sphere-

shaped sub-micron mesoporous silica with a large pore size, which can be scaled up by a facile soft-templating method and is not used vacuum drying, centrifugation and high-cost surfactant like P123 [25–27]. In addition, the comparative investigation was done to determine the effect of cetyltrimethylammonium bromide (CTAB) concentration on textural parameters such as specific surface area, total pore volume and mean pore width and choose the best candidate for drug reservoir and carrier.

## 2. Materials and Methods

### 2.1. Materials

All chemical reagents used to synthesize mesoporous silica were analytical high pure grade. Tetraethyl orthosilicate (TEOS) as the inorganic precursor, cetyltrimethylammonium bromide (CTAB) as the template, and ammonium hydroxide (NH<sub>4</sub>OH, 25 wt% NH<sub>3</sub> in water) as a basic catalyst were purchased from Merck. Additionally, absolute ethanol was supplied from the Zanzan ethanol company (Zanzan, Iran). Also, deionized water was obtained from a water purification system (LAN SHAN, DRo-Di50LS, Iran).

### 2.2. Preparation of mesoporous silica

The mesoporous silica was prepared using the previously reported method for the synthesis of mesoporous bioactive glass with some modifications [28]. Three different amount of CTAB (4.6 mM, 5.9 mM, and 7.2 mM) were entirely dissolved in the mixture of 165 mL deionized water and 78 mL absolute ethanol. 3 mL ammonium hydroxide was added to the above solution. After 30 min stirring, 3 mL TEOS was added. The solution was vigorously stirred for 3 h at room temperature. The resulted suspension was filtered by a filter paper and rinsed with ethanol and deionized water for three times. The collected precipitate was dried at room temperature for 24 h. Finally, the samples were sintered at 650 °C for 3 h (2 °C/min) to remove the organic template. Fig. 1 shows a schematic of the mesoporous silica preparation process.

### 2.3. Characterization of mesoporous silica

The morphology and chemical composition of samples were examined by a field emission scanning electron microscopy (FESEM) coupled to energy dispersive spectrometry (EDS) using MIRA3 FEG-SEM, Tescan. Moreover, The structural characterization was done by X-ray diffraction

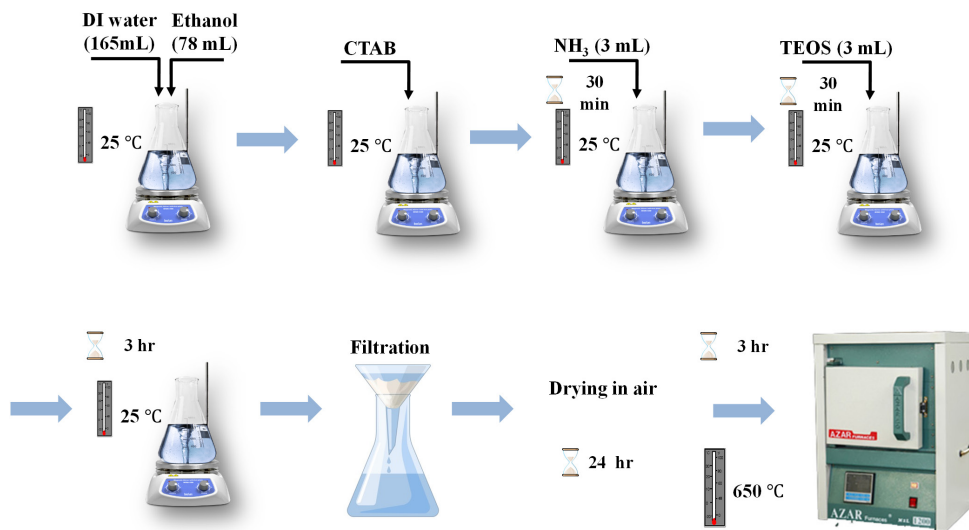


Fig. 1- The schematic of the mesoporous silica preparation process.

(XRD) using PHILIPS PW1730 and Cu-K $\alpha$  radiation generated at 40 kV and 30 mA, in the range of  $2\theta=10-70^\circ$  with the scan rate of  $0.05^\circ$  per second. Functional groups were investigated by Fourier transform infrared (FTIR) spectra in the range of 400-4000  $\text{cm}^{-1}$  with a resolution of 4  $\text{cm}^{-1}$  (BRUKER, Tensor 27, Germany). Furthermore, the specific surface area of samples was measured using multipoint Brunauer–Emmett–Teller (BET) N<sub>2</sub> absorption technique at 77.3 K (BELSORP MINI II, BEL Co., Japan). The BET results were extracted by BEL Japan analysis software. Thermogravimetric analysis (TGA) was done on the dried samples via a TA Instruments Q600 thermal analyzer. The heating rate was 10  $^\circ\text{C}/\text{min}$  and initiated at room temperature up to 650  $^\circ\text{C}$  under air atmosphere.

### 3. Results and discussion

#### 3.1. Textural characterization

Fig. 2 shows the nitrogen adsorption/desorption isotherms of the synthesized samples. According to the IUPAC classification, the adsorption isotherms of samples exhibit the type IV form. Type IV isotherm happens when capillary condensation occurs. Gases condense at a pressure below the gas saturation pressure in the solid's tiny capillary pores. It indicates the formation of a monolayer at the lower pressure areas, followed by the formation of multilayers. This form of isotherm belongs to mesoporous materials with pore diameters between 2-50 nm [29, 30]. As shown in Fig. 2, the adsorption of nitrogen increased gradually at low

pressure. Pores filling from monolayer to multilayer and capillary condensation in the mesopores could also be observed.

There are six types of hysteresis, including H1, H2(a), H2(b), H3, H4, and H5 based on the shape of curves. The type H1 hysteresis could be identified with open ends regular cylindrical shaped porous materials. The type H2 hysteresis loop usually forms in cylindrical-shaped pores with a necking like a bottle. The type H2(a) has a narrower neck than type H2(b). In the H3 type hysteresis, the pores have slit geometry, which results from joining the parallel plate-shaped particles. Moreover, in H4 type hysteresis, the pores have slit-shape but with smaller diameters than H3 type. Finally, H5 type, which is not a very common type, belongs to materials with open mesopores [31, 32]. The difference between these hysteresis curves can be seen in Ref. 31.

In Fig. 2 (4.6 mM and 5.9 mM CTAB) appeared hysteresis phenomenon at  $p/p_0 \approx 1$  assigns to the H3 type which is slit-shape pores. However, in the samples prepared with 7.2 mM CTAB the appeared hysteresis is H4 type. Table 1 presents the textural parameters of the synthesized samples. The results show that increasing the CTAB concentration raises the specific surface area, but for the sample synthesis with 7.2 mM CTAB, increasing the specific surface area is not noticeable. Similarly, the mean pore width has decreased with increasing the surfactant amount. However, total pore volume behaved differently, and the maximum value is

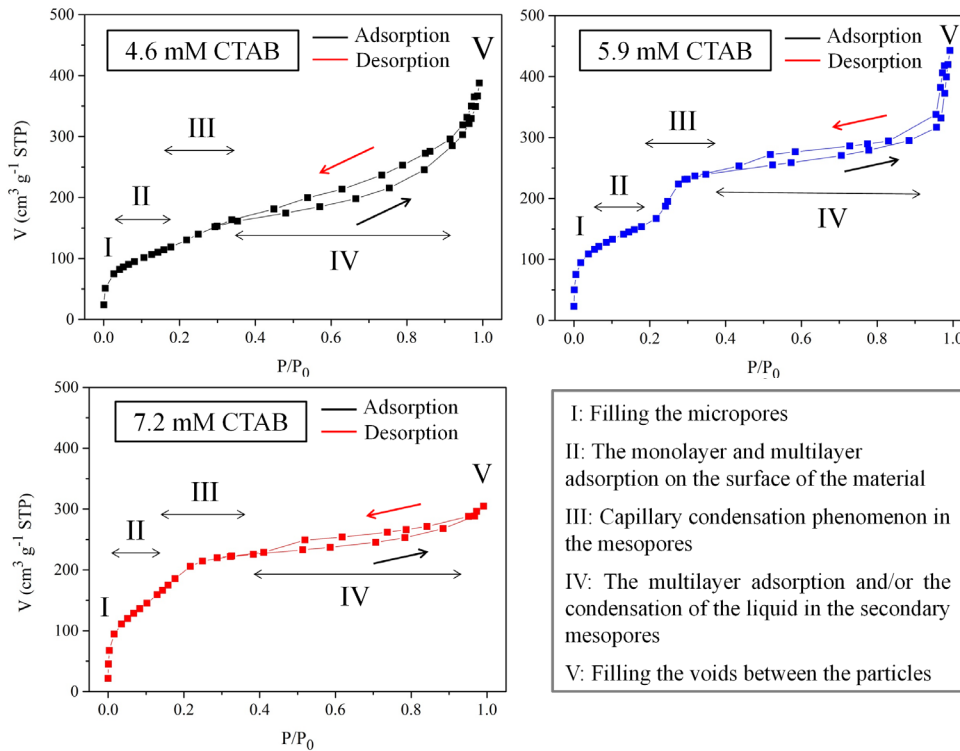


Fig. 2- Nitrogen adsorption/desorption isotherms of the samples.

Table 1- Textural parameters of the samples

Samples	Specific surface area (m <sup>2</sup> g <sup>-1</sup> )	Total pore volume (cm <sup>3</sup> g <sup>-1</sup> )	Mean pore width (nm)
4.6 mM CTAB	416.48	0.5938	5.70
5.9 mM CTAB	535.18	0.6722	5.02
7.2 mM CTAB	564.07	0.4703	3.33

for the sample synthesized with 5.9 mM CTAB. Therefore, according to the obtained results, the sample synthesized with 5.9 mM CTAB is selected as the optimal sample.

### 3.2. Morphology and chemical composition

Fig. 3 displays FESEM images of the samples prepared under different concentrations of CTAB. The FESEM images confirm that the pores of particles are slit-shape. Furthermore, the images show that the sample prepared with 4.6 mM CTAB averagely has large mean pore width, and increasing the CTAB concentration decreases the mean pore width. Moreover, Fig. 4 shows the FESEM image of prepared sample with 5.9 mM CTAB at higher magnification. This image shows that the pores width are almost 5-6 nm. Overall, these images confirm the BET analysis results. Moreover, the results show the average particle size for all samples

is approximately 200 nm.

Fig. 5 reveals the chemical composition of samples synthesized with different concentrations of CTAB. The presence of silicon (Si) and oxygen (O) in all the samples are clear. Considering the percentages of elements and stoichiometric calculations, it can be concluded that the synthesized material in all CTAB concentrations is ~ SiO<sub>2</sub>.

### 3.3. Thermal analysis

To study the calcination process TGA analysis was performed. Also, TGA measurement was conducted to insure the surfactant was removed. Fig. 6 demonstrates the TGA profiles of the fabricated samples. The results show that the total weight loss of prepared samples increases with increasing the CTAB concentration. The first range from 30 to 220 °C relates to loss of water, which is physically adsorbed (from 30 to 120 °C) and condensation of

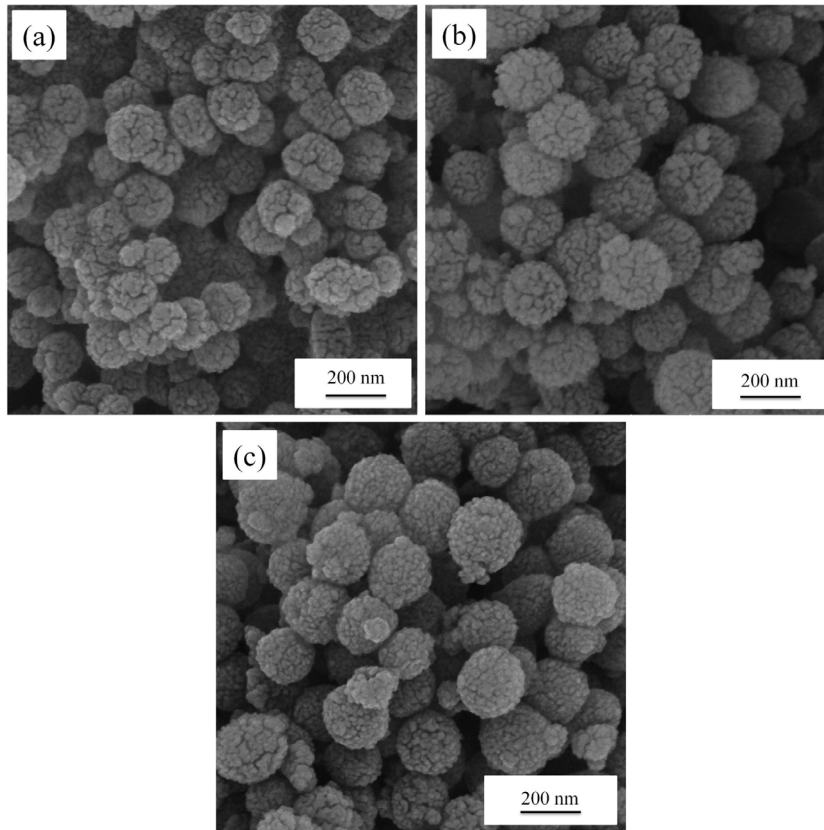


Fig. 3- FESEM micrographs of samples: (a) 4.6 mM CTAB, (b) 5.9 mM CTAB, and (c) 7.2 mM CTAB.

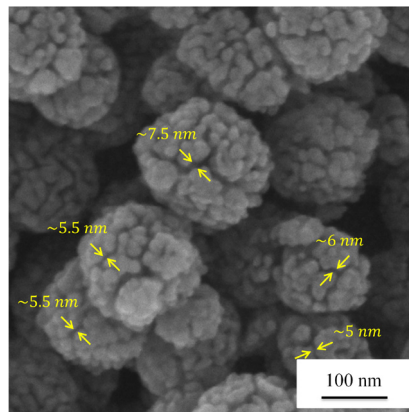


Fig. 4- FESEM image of prepared sample with 5.9 mM CTAB at higher magnification.

silane groups at the surface of samples (from 120 to 220 °C) [33]. In the second range between 220 and 650 °C, the significant weight loss can be seen for all samples, which corresponds to the removal of the remaining CTAB template and alkoxide groups that did not react during the synthesis process. The total weight loss difference can be attributed to the

amount of CTAB in samples. Lu et al. [34] reported 13.8% weight loss for synthesized mesoporous silica with a Pluronic P123 surfactant. Moreover, Zhao et al. [35] synthesized mesoporous silica with cetyltrimethylammonium chloride as a template. The result of TGA analysis shows 58.1 % weight loss which is similar to the results of this study.

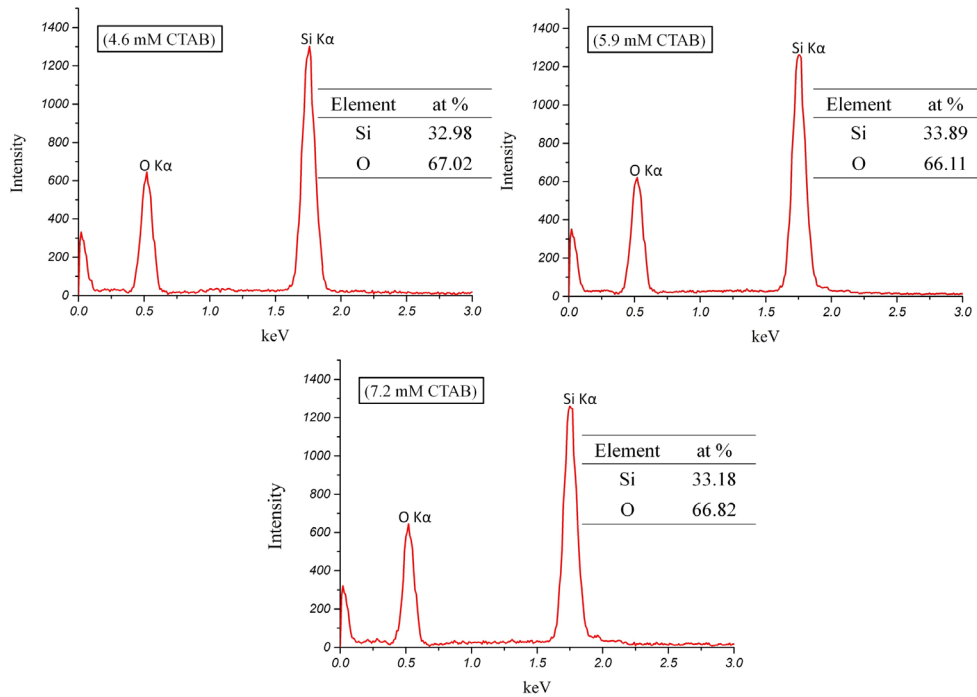


Fig. 5- The elemental composition of samples measured by EDS.

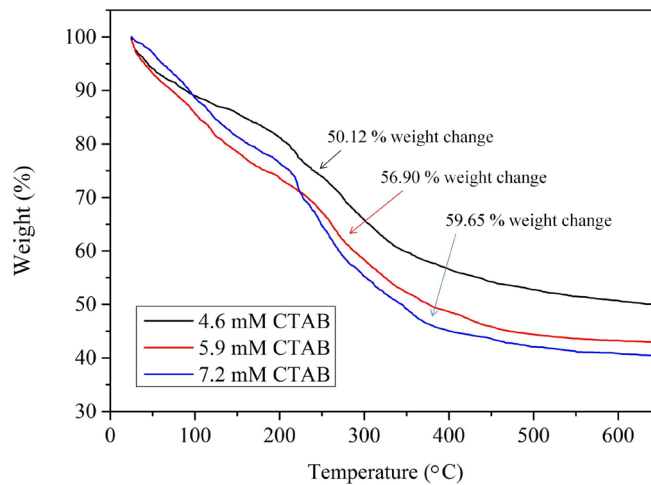


Fig. 6- TGA curves of prepared samples by different concentrations of CTAB.

### 3.4. FTIR spectroscopy

Fig. 7 demonstrates the FTIR analysis of samples synthesized with 5.9 mM CTAB. In this spectrum, the band at 462 cm<sup>-1</sup> corresponds to the deformation mode of Si-O-Si. In addition, the bands at 801 and 1087 cm<sup>-1</sup> attribute to asymmetric stretching vibration and symmetric stretching vibration of Si-O-Si, respectively [36]. Also, the appeared peaks at 1635 and 3434 cm<sup>-1</sup> relate to the

hydroxyl (OH-1) group [37,38]. Besides, the result of FTIR analysis confirms the TGA test results, which shows there are not any bonds related to the surfactant.

### 3.5. XRD analysis

The XRD pattern of mesoporous silica synthesized with 5.9 mM CTAB is shown in Fig. 8. The result exhibits prepared mesoporous silica is

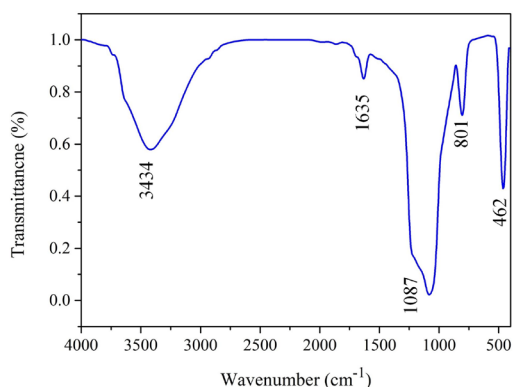


Fig. 7- FTIR spectrum of prepared sample with 5.9 mM CTAB.

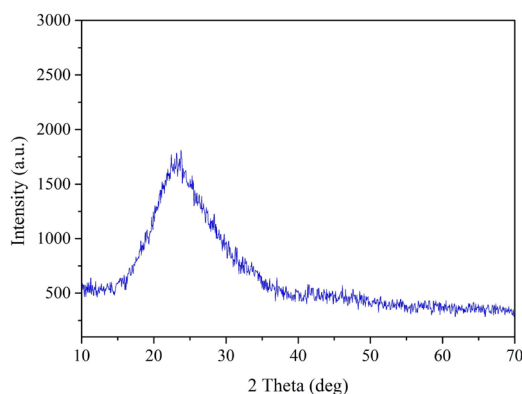


Fig. 8- The XRD pattern of prepared sample with 5.9 mM CTAB.

amorphous. This indicates that even after the heat treating of mesoporous silica at 650 °C for 3 h, the crystallization did not occur. The food and drug administration (FDA) considers the amorphous silica safe. For many years, it has been used in many products or as an excipient in pharmaceutical formulations [39]. It has been reported the mesoporous silica usually shows a bioactive property after 30 days [40]. The bioactivity of these particles depends on the structural parameters and silanol groups as active sites [41]. Furthermore, In the case of biocompatibility, studies have shown that silica has no toxicity on fibroblast cells. The researchers have used different types of mesoporous silica, such as MCM-41 and MCM-48, for drug delivery systems [40]. The investigation of the bioactivity properties and drug release application of these mesoporous particles will be pursued in future works.

#### 4. Conclusions

In the current study, sphere-shaped ultra-fined mesoporous silica successfully synthesized using

cationic surfactant CTAB as a soft template via the sol-gel process. According to the results, the following conclusions can be drawn:

- 1- The BET results reveal the samples have a mesoporous structure with a high specific surface area and total pore volume. Moreover, the textural parameters of samples largely depend on the amount of CTAB concentration.
- 2- The FESEM images exhibit the samples have a relatively homogeneous particle size with the average size of ~200 nm. In addition, both the FESEM images and BET analysis show that the pores have a slit-shape.
- 3- The thermal analysis demonstrates that increasing the amount of CTAB causes to increase the total weight loss. Weight loss relates to the evaporation of absorbed water, condensation of silane groups, the removal of remaining CTAB template and alkoxide groups. However, crystallization does not occur up to 650 °C.
- 4- The EDS, FTIR, and XRD results show that the prepared samples have an amorphous SiO<sub>2</sub> structure.

#### References

1. Vallet-Regí M, Balas F, Arcos D. Mesoporous Materials for Drug Delivery. *Angewandte Chemie International Edition*. 2007;46(40):7548-58.
2. Vallet-Regí M. Ordered Mesoporous Materials in the Context of Drug Delivery Systems and Bone Tissue Engineering. *Chemistry - A European Journal*. 2006;12(23):5934-43.
3. Wang Y, Zhao Q, Han N, Bai L, Li J, Liu J, et al. Mesoporous silica nanoparticles in drug delivery and biomedical applications. *Nanomedicine: Nanotechnology, Biology and Medicine*. 2015;11(2):313-27.
4. Scott BJ, Wirnsberger G, Stucky GD. Mesoporous and Mesostructured Materials for Optical Applications. *Chemistry of Materials*. 2001;13(10):3140-50.
5. Li W, Liu J, Zhao D. Mesoporous materials for energy conversion and storage devices. *Nature Reviews Materials*. 2016;1(6).
6. Corma A, Moliner M, Díaz-Cabañas MJ, Serna P, Femenia B, Primo J, et al. Biomimetic synthesis of microporous and mesoporous materials at room temperature and neutral pH, with application in electronics, controlled release of chemicals, and catalysis. *New Journal of Chemistry*. 2008;32(8):1338.
7. Vallet-Regí M, Ruiz-González L, Izquierdo-Barba I, González-Calbet JM. Revisiting silica based ordered mesoporous materials: medical applications. *J Mater Chem*. 2006;16(1):26-31.
8. Giri S, Trewyn BG, Lin VSY. Mesoporous silica nanomaterial-based biotechnological and biomedical delivery systems. *Nanomedicine*. 2007;2(1):99-111.
9. Ariga K, Vinu A, Yamauchi Y, Ji Q, Hill JP. Nanoarchitectonics

- for Mesoporous Materials. *Bulletin of the Chemical Society of Japan*. 2012;85(1):1-32.
10. Soler-Illia GJAA, Azzaroni O. Multifunctional hybrids by combining ordered mesoporous materials and macromolecular building blocks. *Chemical Society Reviews*. 2011;40(2):1107.
  11. Liu J, Qiao SZ, Hu QH, Max Lu GQ. Magnetic Nanocomposites with Mesoporous Structures: Synthesis and Applications. *Small*. 2011;7(4):425-43.
  12. Ciesla U, Schüth F. Ordered mesoporous materials. *Microporous and Mesoporous Materials*. 1999;27(2-3):131-49.
  13. Bao Y, Shi C, Wang T, Li X, Ma J. Recent progress in hollow silica: Template synthesis, morphologies and applications. *Microporous and Mesoporous Materials*. 2016;227:121-36.
  14. Farjadian F, Roointan A, Mohammadi-Samani S, Hosseini M. Mesoporous silica nanoparticles: Synthesis, pharmaceutical applications, biodistribution, and biosafety assessment. *Chemical Engineering Journal*. 2019;359:684-705.
  15. Pal N, Bhaumik A. Soft templating strategies for the synthesis of mesoporous materials: Inorganic, organic-inorganic hybrid and purely organic solids. *Advances in Colloid and Interface Science*. 2013;189-190:21-41.
  16. Ying JY, Mehnert CP, Wong MS. Synthesis and Applications of Supramolecular-Templated Mesoporous Materials. *Angewandte Chemie International Edition*. 1999;38(1-2):56-77.
  17. Wan Y, Zhao. On the Controllable Soft-Templating Approach to Mesoporous Silicates. *Chemical Reviews*. 2007;107(7):2821-60.
  18. Vartuli JC, Kresge CT, Leonowicz ME, Chu AS, McCullen SB, Johnson ID, et al. Synthesis of Mesoporous Materials: Liquid-Crystal Templating versus Intercalation of Layered Silicates. *Chemistry of Materials*. 1994;6(11):2070-7.
  19. Slowing I, Viveroescoto J, Wu C, Lin V. Mesoporous silica nanoparticles as controlled release drug delivery and gene transfection carriers. *Advanced Drug Delivery Reviews*. 2008;60(11):1278-88.
  20. Vivero-Escoto JL, Slowing II, Trewyn BG, Lin VSY. Mesoporous Silica Nanoparticles for Intracellular Controlled Drug Delivery. *Small*. 2010;6(18):1952-67.
  21. Vallet-Regí M, Rámila A, del Real RP, Pérez-Pariente J. A New Property of MCM-41: Drug Delivery System. *Chemistry of Materials*. 2001;13(2):308-11.
  22. Shi X, Wang Y, Wei K, Ren L, Lai C. Self-assembly of nanohydroxyapatite in mesoporous silica. *Journal of Materials Science: Materials in Medicine*. 2008;19(8):2933-40.
  23. Croissant JG, Fatieiev Y, Khashab NM. Degradability and Clearance of Silicon, Organosilica, Silsesquioxane, Silica Mixed Oxide, and Mesoporous Silica Nanoparticles. *Advanced Materials*. 2017;29(9):1604634.
  24. Yang Y, Li J. Silica-based Nanostructured Porous Biomaterials. *Advanced Topics in Science and Technology in China: Springer Berlin Heidelberg*; 2010. p. 1-30.
  25. Li X, Garamus VM, Li N, Gong Y, Zhe Z, Tian Z, et al. Preparation and characterization of a pH-responsive mesoporous silica nanoparticle dual-modified with biopolymers. *Colloids and Surfaces A: Physicochemical and Engineering Aspects*. 2018;548:61-9.
  26. Martínez-Carmona M, Lozano D, Colilla M, Vallet-Regí M. Lectin-conjugated pH-responsive mesoporous silica nanoparticles for targeted bone cancer treatment. *Acta Biomaterialia*. 2018;65:393-404.
  27. Rosenholm JM, Zhang J, Sun W, Gu H. Large-pore mesoporous silica-coated magnetite core-shell nanocomposites and their relevance for biomedical applications. *Microporous and Mesoporous Materials*. 2011;145(1-3):14-20.
  28. Hu Q, Li Y, Zhao N, Ning C, Chen X. Facile synthesis of hollow mesoporous bioactive glass sub-micron spheres with a tunable cavity size. *Materials Letters*. 2014;134:130-3.
  29. Hwang N, Barron AR. BET surface area analysis of nanoparticles. *The Connexions project*. 2011:1-1.
  30. Zheng X, Zhang J, Wang J, Qi X, Rosenholm JM, Cai K. Polydopamine Coatings in Confined Nanopore Space: Toward Improved Retention and Release of Hydrophilic Cargo. *The Journal of Physical Chemistry C*. 2015;119(43):24512-21.
  31. Oliveira DM, Andrada AS. Synthesis of ordered mesoporous silica MCM-41 with controlled morphology for potential application in controlled drug delivery systems. *Cerâmica*. 2019;65(374):170-9.
  32. Thommes M, Kaneko K, Neimark AV, Olivier JP, Rodriguez-Reinoso F, Rouquerol J, et al. Physisorption of gases, with special reference to the evaluation of surface area and pore size distribution (IUPAC Technical Report). *Pure and Applied Chemistry*. 2015;87(9-10):1051-69.
  33. Tabia Z, El Mabrouk K, Bricha M, Nouneh K. Mesoporous bioactive glass nanoparticles doped with magnesium: drug delivery and acellular in vitro bioactivity. *RSC Advances*. 2019;9(22):12232-46.
  34. Lu B, Kawamoto K. A novel approach for synthesizing ordered mesoporous silica SBA-15. *Materials Research Bulletin*. 2012;47(6):1301-5.
  35. Zhao XS, Lu GQ, Whittaker AK, Millar GJ, Zhu HY. Comprehensive study of surface chemistry of MCM-41 using <sup>29</sup>Si CP/MAS NMR, FTIR, pyridine-TPD, and TGA. *The Journal of Physical Chemistry B*. 1997 Aug 14;101(33):6525-31.
  36. Jani AT, Haghighi NB, Sheikh Hossein Pour M, Aminian M, Molzemi S. Hydroxyapatite incorporation into MCM-41 and study of ibuprofen drug release. *Journal of the Australian Ceramic Society*. 2019;56(2):653-61.
  37. Xu H, Ge Y-W, Lu J-W, Ke Q-F, Liu Z-Q, Zhu Z-A, et al. Icarin loaded-hollow bioglass/chitosan therapeutic scaffolds promote osteogenic differentiation and bone regeneration. *Chemical Engineering Journal*. 2018;354:285-94.
  38. Koohkan R, Hooshmand T, Tahriri M, Mohebbi-Kalhari D. Synthesis, characterization and in vitro bioactivity of mesoporous copper silicate bioactive glasses. *Ceramics International*. 2018;44(2):2390-9.
  39. Juère E, Kleitz F. On the nanopore confinement of therapeutic drugs into mesoporous silica materials and its implications. *Microporous and Mesoporous Materials*. 2018;270:109-19.
  40. Wang S. Ordered mesoporous materials for drug delivery. *Microporous and Mesoporous Materials*. 2009;117(1-2):1-9.
  41. Vallet-Regí M. Nanostructured mesoporous silica matrices in nanomedicine. *Journal of Internal Medicine*. 2010;267(1):22-43.